The International Journal of Advanced Manufacturing Technology (2020) 108:1039–1048
https://doi.org/10.1007/s00170-019-04672-4

ORIGINAL ARTICLE

Generation of microcones on reaction-bonded silicon carbide by nanosecond pulsed laser irradiation

Tushar Meshram[1] · Jiwang Yan[1]

Received: 31 May 2019 / Accepted: 5 November 2019 / Published online: 16 December 2019

Abstract
Silicon carbide (SiC) is heavily used in the industry due to its resistance to chemical wear and excellent mechanical properties such as high hardness and high stiffness. However, these properties make it difficult to produce micro and nanostructures on the surface of SiC by conventional methods. In this study, high-density microcones that protrude ~ 10 μm above the initial surface have been fabricated by nanosecond pulsed Nd:YAG laser irradiation (λ = 532 nm) on reaction-bonded SiC. Geometrically aligned cones were also fabricated by modifying the laser scanning path, and effect of different parameters such as pulse frequency, laser fluence was studied. It was observed that the surface morphology of microcones was affected by the pulse width and beam overlap. X-ray spectroscopy and Raman spectroscopy showed that the microcones were mainly composed of silicon. Formation of these cone structures made the surface highly superhydrophilic with a contact angle of ~ 0°.

Keywords Laser irradiation · Reaction-bonded silicon carbide · Surface texturing · Microcone · Superhydrophilic surface

1 Introduction

Reaction-bonded silicon-carbide (RB-SiC), due to its unique properties such as high hardness, high stiffness, imperviousness to chemical attacks, and high dimensional stability, is seen as a promising material for anti-wear parts, mechanical seals, and precision components. In addition, RB-SiC is also lightweight and has high thermal conductivity and low thermal expansion; therefore, it can be used in mechanical systems that must work in harsh environments. One such application is outer space optical devices such as mirrors and reflectors [1, 2]. Other applications include high-precision optical molds, rolling bearings, and cutting tools. Microstructuring the RB-SiC surface can enhance surface properties, such as wettability, reflectivity, and friction coefficient, and, in turn, improve functionality of these applications.

Properties which make RB-SiC an excellent engineering material also makes it difficult to machine. RB-SiC is harder than most machining tool materials, and only a few tool materials can be used to machine RB-SiC, such as diamond and cubic boron nitride, which make processing RB-SiC very costly. In addition, RB-SiC is a two-phase material which consists of SiC grains bonded by Si matrix. Si and SiC have different mechanical and chemical properties, which make it difficult to generate uniform microstructure on the surface by mechanical or chemical processes.

Laser processing can be used to create microstructures on the surface to enhance surface properties [3]. Laser accomplishes this by modifying the surface locally without altering the properties of bulk material. Microstructures generated by laser have been known to improve tribological properties. Serguei and Murzin reported that the coefficient of friction was reduced after microstructure formation on rolling bearings made from SiC [4]. Microstructure can also improve the thickness of lubricant film, thus improving the load-carrying capacity of bearing under hydrodynamic sliding condition [5]. Silicon microcones and nanograss produced by cryogenic deep reactive ion etching made the surface superhydrophobic [6]; such surface can be used as self-cleaning [7] or for improving laminar flow enhancement. On the other hand, hydrophilic surface can be used in heat transfer applications; spreading of water increases the surface area between surface and water increasing heat transfer. Formation of silicon microcones is also known to improve absorption of near-infrared radiation significantly [8, 9].

✉ Jiwang Yan
yan@mech.keio.ac.jp

[1] Department of Mechanical Engineering, Keio University, Yokohama, Japan

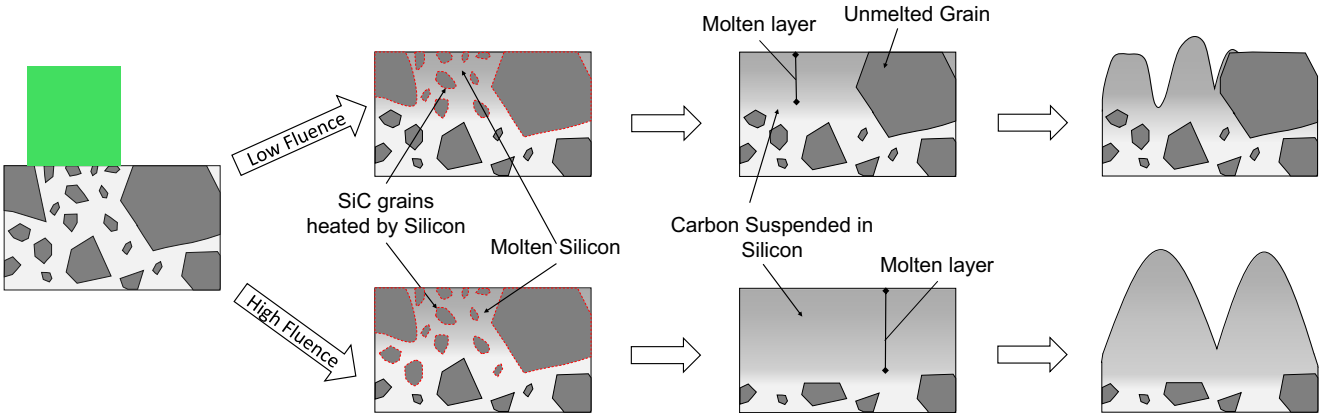

Fig. 1 Schematic of cone formation mechanism at various laser fluences

In this paper, we propose an innovative method for fabricating conical microstructure on the surface of RB-SiC by nanosecond pulsed laser irradiation. This method takes advantage of the difference in material properties of Si and SiC components and responses to laser irradiation. The shape, height, and material composition of the conical structures were investigated under various conditions. In addition, we also examined the contact angle with water to investigate effect of microstructure formation on surface wettability.

2 Process mechanisms

2.1 Interaction of laser with RB-SiC

In semiconductors, absorption of laser photons primarily occurs by excitation of an electron from valance band to the conduction band or intersubband transition of electron [10]. Photons with energy below the band gap are not absorbed. These low energy photons can be absorbed if impurities are present in the material or by multiphoton absorption [11]. RB-SiC is a two-phase material consisting of SiC grains bonded by Si [12]. Silicon has a band gap of 1.1 eV, while 6H-SiC is a wide-band gap semiconductor with an indirect band gap of 3.023 eV at 300 K [13] (2.86 eV [14]), corresponding to a wavelength of 413 nm which is shorter than the wavelength of the laser (532 nm, 2.33 eV) used in this study. The bandgap of semiconductors decreases with increase in temperature. Groth and Kauer reported the absorption coefficient of 6H-SiC at 293 K was negligible for photons with wavelength of 532 nm [15]. Watanabe et al. reported that even at elevated temperature of 573 K, absorption coefficient of 6H-SiC was negligible [16]. Choyke et al. reported the rate of change of energy gap with temperature above 300 K as described in Equation (1), and Levinshtein reported Equation (2) for energy gap calculation [17, 18]:

$$\frac{dE_g}{dT} = -3.3*10^{-4}*T \tag{1}$$

$$E_{g(T)} = E_{g(0)} - 6.5*10^{-4}\left(\frac{T^2}{T+1200}\right) \tag{2}$$

where E_g is energy gap and T is temperature in Kelvin. Equation (1) and Equation (2) were used to obtain temperature at which band gap of 6H-SiC reduces to 2.33 eV. Calculated temperature was 1900 K from Equation (1) and 1800 K from Equation (2). It can thus be assumed that 6H-SiC grain cannot directly absorb 532 nm wavelength laser at room temperature (300 K). However, band gap of silicon is 1.1 eV at room temperature; thus, it can absorb laser. This results in selective heating of silicon by laser, which heats the SiC grains by conduction. As the temperature of SiC grains increases, the absorption coefficient will increase for photons with energy of 2.33 eV.

2.2 Mechanism of cone formation

It is known that laser irradiation in air can cause thermal decomposition of silicon carbide into silicon and carbon [19–21]. Furthermore, laser oxidizes silicon and carbon [22, 23].

In air : $SiC_{(s)} \rightarrow Si_{(l)} + C_{(s)}$

$2SiC_{(s)} + 2O_2 \rightarrow 2SiO + 2C_{(s)}$

Table 1 Laser parameters

	Area scanning	Spot irradiation
Wavelength (nm)	532	532
Spot size (μm)	85	85
Pulse width (ns)	48.4	15.6 48.4
Frequency (kHz)	10	1, 10
Scanning speed (mm/s)	10	-
Fluence (J/cm^2)	1.58, 2.11, 3.17, 4.22	3.17–14
Number of pulse	-	5–50, 50–500
Pitch(μs)	10	-

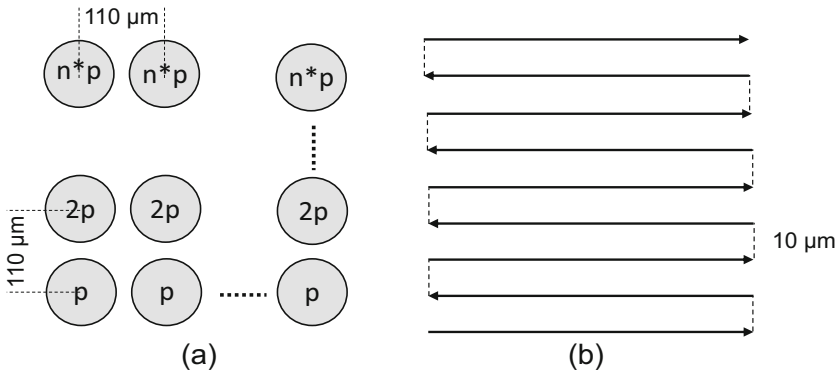

Fig. 2 Laser scanning scheme. **(a)** Spot irradiation. **(b)** Area irradiation

$$2SiO + 2O_2 \rightarrow 2SiO_{2(s)}$$

$$C_{(s)} + O_2 \rightarrow CO_2$$

Several researchers have reported that laser irradiation on SiC formed a layer of silicon on the surface [22–24]. Silicon melts at a much lower temperature (1687 K) as compared to silicon carbide (3103 K); hence, different mechanisms are considered for low and high fluence. This provides possibility of cone formation on RB-SiC by laser irradiation.

Figure 1 shows the schematic of possible cone formation on RB-SiC by laser irradiation. At low fluence, silicon is directly heated and melted by laser. However, SiC cannot absorb laser directly as the band gap of SiC is larger than the laser photon energy. Instead, SiC grains are indirectly heated by Si. At low fluence, high temperatures of Si cannot be sustained for longer duration; hence, only smaller SiC grains are melted, whereas larger grains are less affected. Thus melt pool is formed in between larger SiC grains. SiC melts into a pool of carbon suspended in liquid silicon [19–21, 25]. Due to plasma recoil pressure, the molten mixture is pushed upwards, which then cools rapidly, forming conical structures. Conical structures are aligned with laser propagation direction. Low fluence condition can be used to specifically generate cones in areas where large SiC grains are not present.

At high fluence, silicon is rapidly heated to very high temperature; for the same laser scan speed (or pulse overlap), this elevated temperature can be sustained for a longer time. Thus at high fluence condition, even larger SiC grains are melted. In addition, the depth of melt pool formed is also substantial. The material is pushed much higher above the initial surface due to the larger volume of molten mixture and higher plasma recoil pressure, which cools rapidly forming conical structures. The cones generated at high fluence have a larger base diameter and protrude above the initial surface. At high fluence, the conical structures are generated on the entire surface.

3 Experimental methods

3.1 Laser systems

Two different lasers were used in this study for comparison: LR-SHG laser (Nd:YAG laser) from Mega Opto Co., Ltd., Japan (Laser 1) and Super pulse 532-30 (Nd:YVO_4 laser)

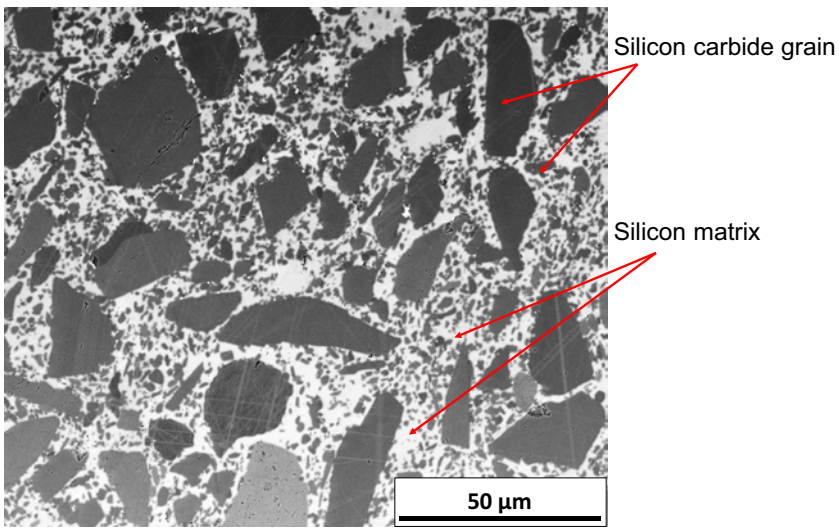

Fig. 3 SEM images of sample surface after polishing

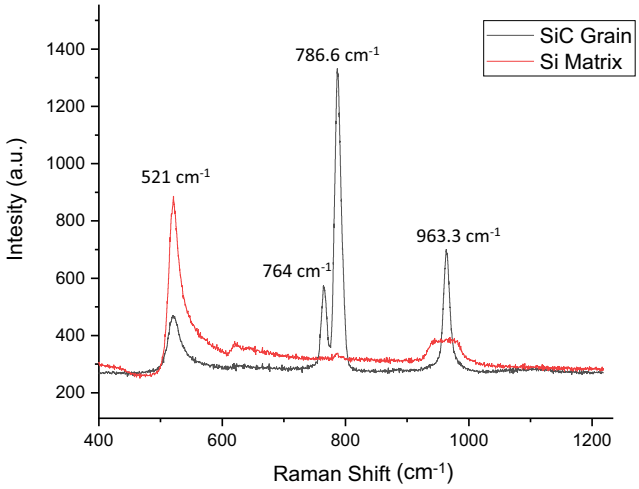

Fig. 4 Raman spectra of SiC grains and Si matrix

from Suzhou Inngu Laser Co., Ltd., China (Laser 2). Both of the lasers were linearly polarized with a wavelength of 532 nm, and spot diameter was 85 μm with a Gaussian distribution. Laser 1 has a pulse frequency range of 1 kHz to 10 kHz with pulse width of 15.6 ns and 48.4 ns, respectively, while Laser 2 laser has a pulse frequency range of 70 kHz to 150 kHz with pulse width of 19 ns and 38 ns, respectively.

The laser beam scanning was controlled using a galvanometer scanner system. The sample was directly placed on the stage, and laser was focused onto the workpiece using an f-theta lens. Experiments were carried in atmospheric conditions. Laser parameters are shown in Table 1. For spot irradiation, laser was irradiated in a grid of 10 × 10 spots with a pitch of 110 μm in *x* and *y*-direction. In *x*-direction number of pulses, p were kept constant to remove effect of local surface microstructure. In *y*-direction, number of pulse were increased by a factor of n, where n is the row number as shown in Fig. 2a. Figure 2b shows laser scanning path for area irradiation, laser beam was irradiated in a line, then the laser beam was moved transversely at a pitch of 10 μm, and the second line was irradiated in the opposite direction. This line scan was repeated to cover a set area.

3.2 RB-SiC sample

The RB-SiC samples used in this experiment were cylindrical with a diameter of 70 mm and height 15 mm. The surface was flat with a roughness of Ra 0.18 μm. To examine the distribution of SiC grains in the Si matrix, a sample was polished to a mirror finish. Figure 3 shows an SEM micrograph of the sample surface where SiC grains (black) and Si matrix (white) can be identified. Raman spectroscopy was performed to characterize the material structures. Figure 4 shows the obtained Raman spectrum. The SiC grains showed a Raman shift for single-crystal 6H-SiC (α-SiC) and the Si matrix for single-crystal Si. The average size of larger grains was around 50 μm. Most of the large SiC grains are not directly bonded to each other; silicon and smaller SiC grains exist in between them.

3.3 Surface measurement and analysis

After laser irradiation, the surface was cleaned with ethanol, and generated microstructure was observed using a scanning electron microscope (SEM), and surface topography was measured by a laser microscope. Energy-dispersive X-ray (EDAX) spectroscopy and Raman spectroscopy were performed to study the material composition of the surface. SImage Entry 5 made by Excimer Inc. was used to measure the contact angle of water with surface after cone generation.

4 Results and discussion

4.1 Effect of pulse width and frequency

Spot irradiation was carried out to observe the effect of laser pulse width. Figure 5a shows spot irradiation results where pulse frequency was 1 kHz and pulse width was 15.6 ns. It was observed that cones did not form instead a shallow hole with a rim was formed. There are two reasons for this: first, pulse width is small to cause significant melting. Second, the

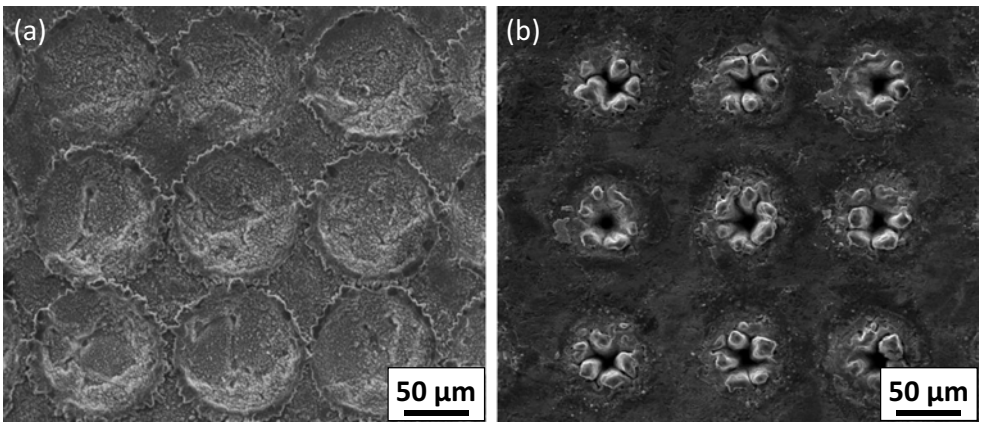

Fig. 5 SEM image of point irradiation with **(a)** 15.6 ns and **(b)** 48.4 ns

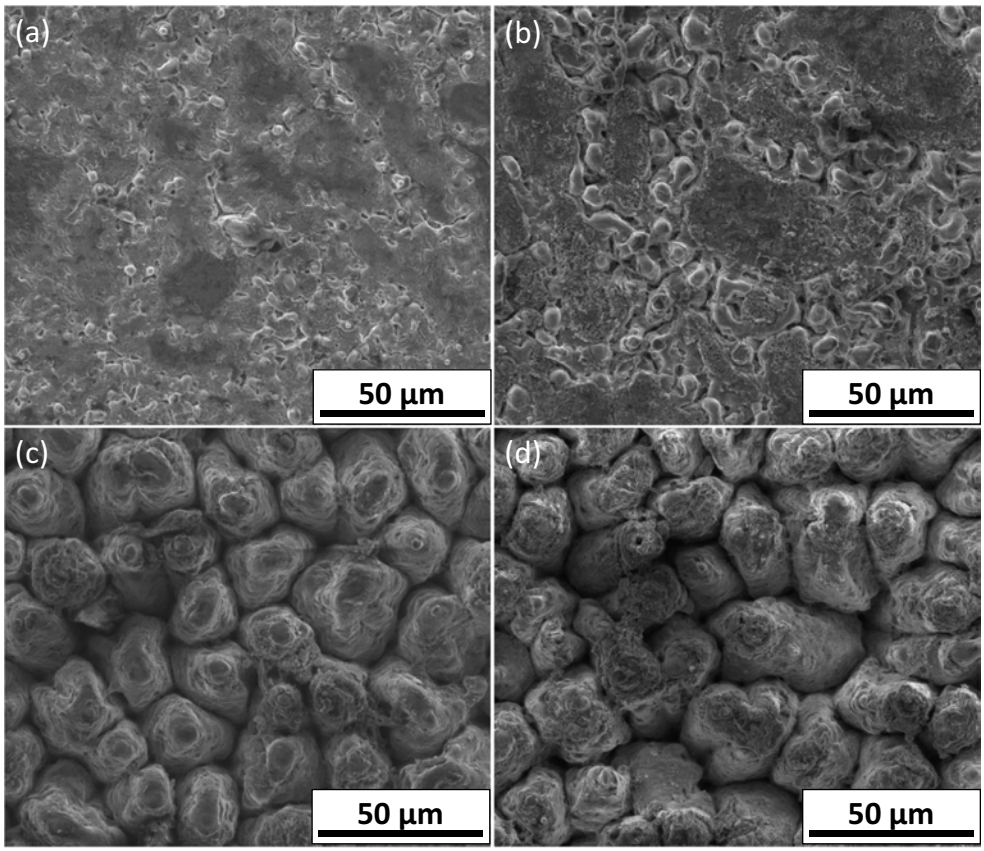

Fig. 6 SEM images of area irradiation with fluence of **(a)** 1.58, **(b)** 2.11, **(c)** 3.17, and **(d)** 4.22 J/cm^2

time difference between two subsequent pulses is long, hence negligible plasma shielding occurs, which results into no or very weak plasma formation, i.e., the pulse frequency is not enough for generating strong plasma which could force the molten material upwards. But due to temperature gradient created by Gaussian, beam material is pushed towards the edge due to thermocapillary flow [26]. Figure 5b shows spot irradiation results where pulse frequency was 10 kHz and laser pulse width was 48.4 ns. It can be seen in Fig. 5b that small conical structures formed on the surface. Formation of similar structure was attributed to material movement due to laser-induced plasma recoil pressure [27]. Cones are generated because longer pulse can melt more material and high frequency creates higher recoil pressure, thus forcing molten material upwards. Furthermore, at a higher frequency, the time duration between two consecutive pulses is shorter. Thus, restricting the amount of heat diffusion occurs between consecutive pulses. Hence at a high frequency, high temperature can be sustained for a more extended time [28], which helps in maintaining the material in molten state and also provides time for this molten material to be transported above the initial surface. It can thus be asserted that for a given set of irradiation conditions, increasing frequency will improve cone formation until the max temperature achieved exceeds the vaporization temperature of Si substantially as it will lead to ablation.

4.2 Effect of fluence

Area irradiation at different fluence was carried out to understand the effect of fluence on conical microstructure formation. Scanning scheme mentioned in method section was used with a laser scan speed of 10 mm/s and scanning repetition of 5; pulse width of 48.4 ns and pulse frequency 10 kHz. Figure 6 shows SEM images of structures formed at fluence of 1.58, 2.11, 3.17, and 4.22 J/cm^2.

At very low fluence (1.58 J/cm^2), only small volume of the silicon is melted and is pushed out on the surface. The plasma pressure is not enough to push molten silicon much above initial surface, thus forming small bump-shaped structures (Fig. 6a). The unaffected areas are thought to be large SiC grains.

At low fluence (2.11 J/cm^2), the dome-shaped structures (Fig. 6b) are formed in the areas with small SiC grains. These structures have a small base diameter and are more in number; this is because the volume of melt pool is small and plasma pressure is not enough to cause large displacement of molten material which would force them to combine and form larger cones.

At high fluence (3.17 J/cm^2), even larger SiC grains can be melted; hence, conical structures are formed on the entire surface (Fig. 6c). The cones formed have large base diameter and height. In addition, cones also have smooth tips with very less reattached debris. It is hypothesized that sizes of cones are

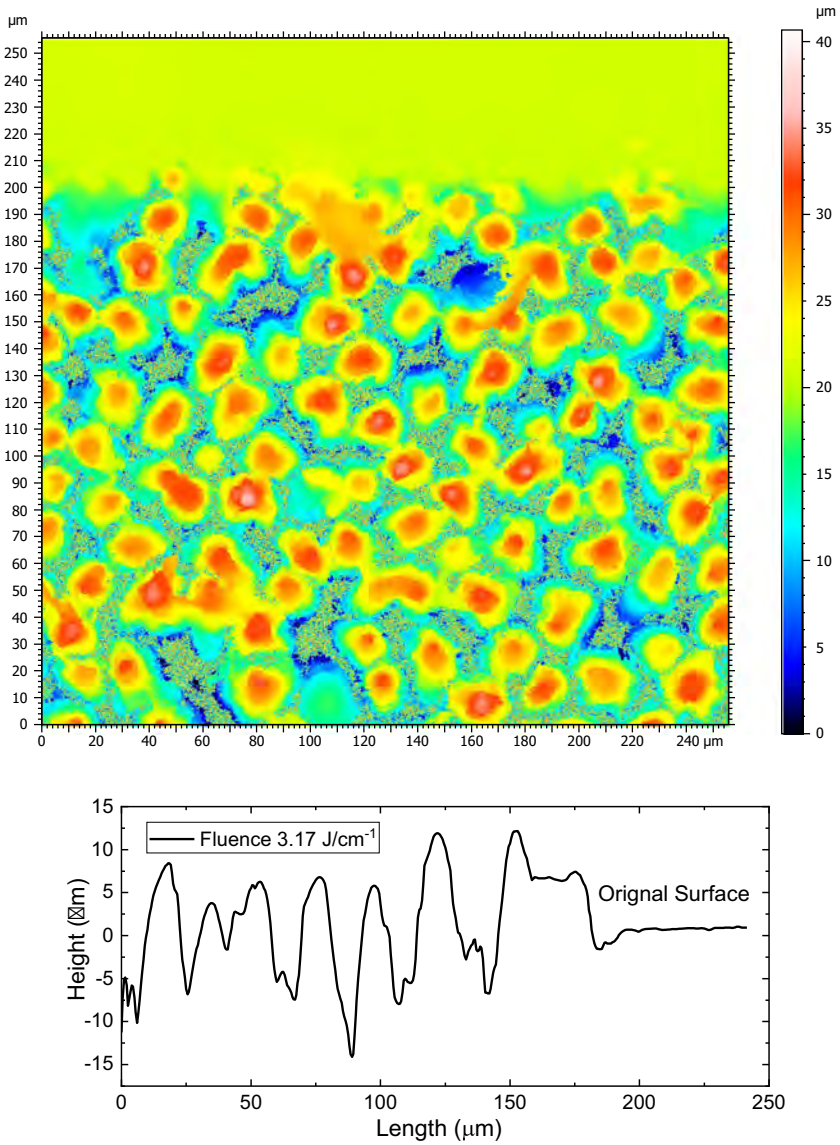

Fig. 7 Surface topography at a fluence of 3.17 J/cm^2

large because the volume of melt pool is more substantial and plasma pressure can push molten material well above the initial surface. Figure 7 shows surface topography of generated cones. Green area on the top is unirradiated surface, and the red spots on the bottom are peaks of cones generated after laser irradiation.

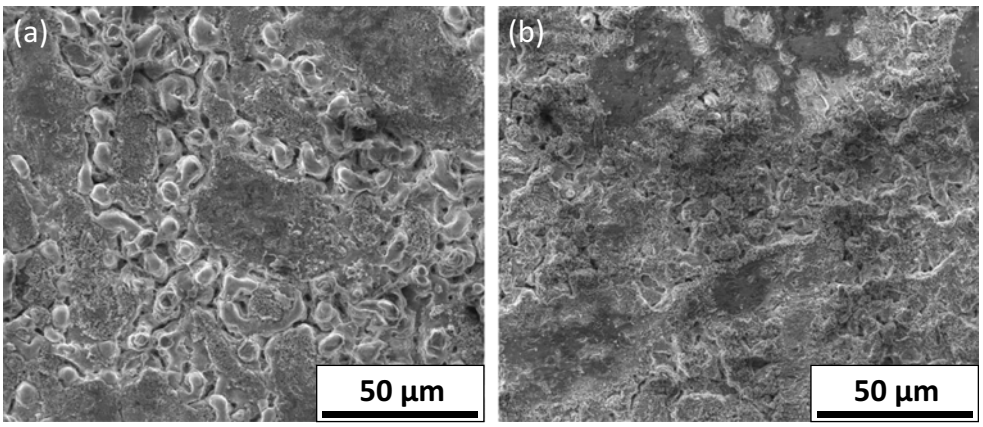

Fig. 8 SEM image of area irradiation with scanning repetition of **(a)** 5 and **(b)** 20

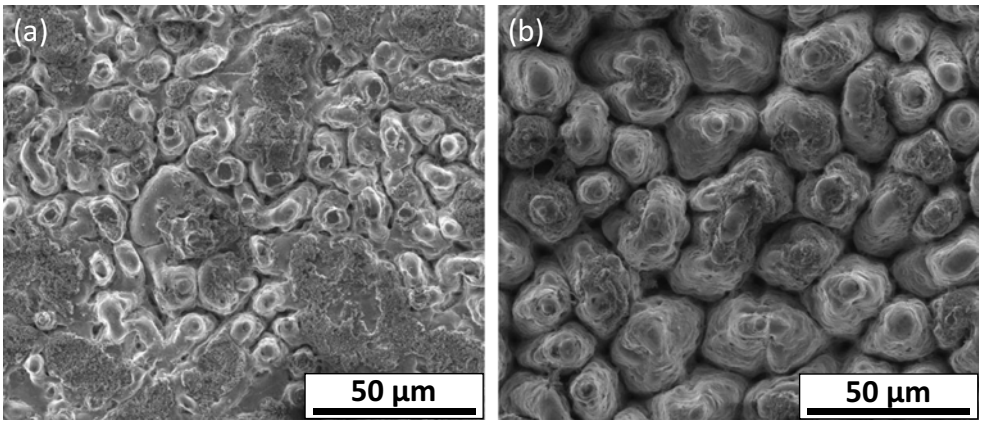

Fig. 9 SEM images of area irradiation with fluence of **(a)** 3.17 J/cm^2 and **(b)** 4.22 J/cm^2

At very high fluence (4.22 J/cm^2), it was expected that even larger cones as compared to high fluence condition will form. However, the conical structures generated were of similar size. In addition, the surface of cones was covered with reattached debris, which can be observed in Fig. 6d. This is because an increase in laser fluence will increase the amount of silicon vaporization. It is hypothesized that while some of the vaporized silicon gets deposited on the surface, most of it is ablated.

4.3 Effect of scanning repetition

Area irradiation was performed with a different number of scanning repetition. SEM images of the irradiated surface at the repetition of 5 and 20 are shown in Fig. 8. In 5-time repetition, small conical structure can be observed, whereas in 20-time repetition, it was expected that larger cones will form; however, cones are not present, and instead a porous layer of splattered material can be seen on the surface. Generated cones are mostly made up of silicon, hence scanning laser again on cones causes silicon to vaporize and get splatter on the surface. For laser pulse fluence 3.17 J/cm^2, optimum number of scanning repletion is 5 (Fig. 6c). However, at laser pulse fluence of 4.22 J/cm^2 and scanning repletion of 5, we can observe some ablation of cone peaks and deposition of vaporized silicon on the surface (Fig. 6d).

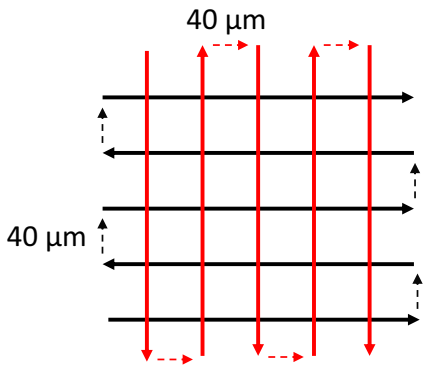

Fig 10 Scanning path for grid pattern irradiation

Thus, at higher fluence, number of scanning repetition should be reduced to avoid ablation and adhesion of silicon.

4.4 Effect of laser scan speed

In this section, we investigate the effect of laser scanning speed on the formation of conical structures. From previous sections, we know that at higher fluence, multiple scanning repetition leads to ablation of already generated microcones. Hence in this experiment to reduce ablation at higher repetition rate, we increased scan speed with each scanning repetition. Area irradiation was carried out with the scanning scheme shown in Fig. 2b and scanning repetition of 5. Other laser parameters are shown in Table 1. The initial scan speed was 10 mm/s, and after every scanning repetition, the scan speed was increased by 10 mm/s, i.e., second scanning repetition was carried with speed of 20 mm/s and third with 30 mm/s and so on.

We can clearly observe that the microstructure formation at 3.17 J/cm^2 in Fig. 9a is similar to Fig. 6b, where fluence was 2.11 J/cm^2. Similarly, conical structures at 4.22 J/cm^2 in Fig. 9b are similar to Fig. 6c where fluence was 3.17 J/cm^2. This means that the effect of increasing scan speed is similar to that of decreasing pulse fluence. When scan speed increases, the pulse overlap decreases which in turn leads to a lower temperature rise in RB-SiC [28]. Furthermore, it reduces the amount of time for which this temperature can be sustained in irradiated region. Hence, increasing scan speed shifts the fluence at which cones can be generated to a higher value.

Table 2 Laser parameters for cross irradiation

Wavelength [nm]	532
Spot size [µm]	85
Pulse width [ns]	30
Frequency [kHz]	100
Scanning speed [mm/s]	60
Fluence [J/cm^2]	1.76
Pitch[µs]	40

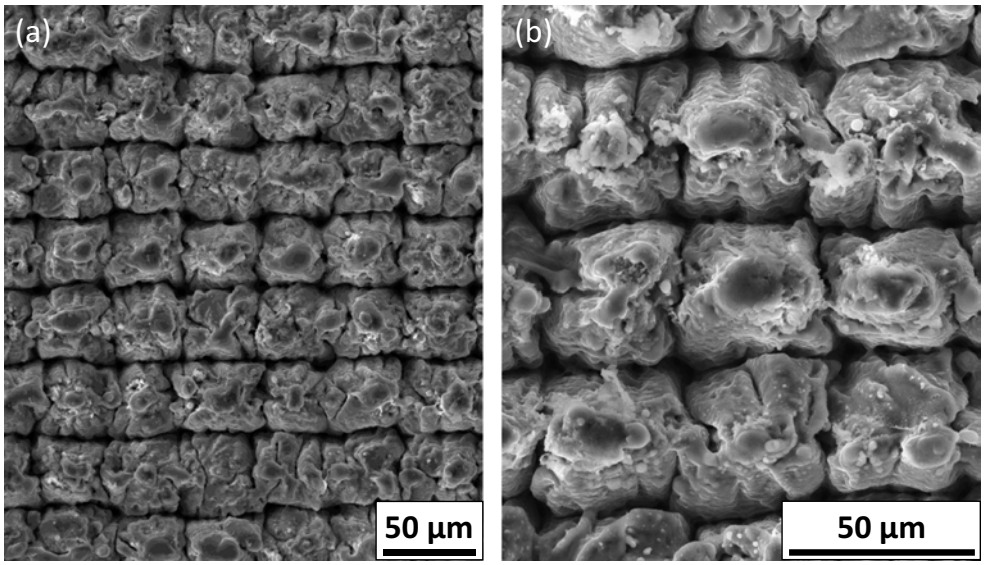

Fig. 11 SEM image of cross irradiation

4.5 Geometrically patterned cone formation

The formation mechanism of cones is dependent on the melting of surface and movement of the molten material due to plasma recoil pressure. Hence in order to control the location of cone formation, we used a laser with a high pulse frequency of 100 kHz. This results in generation of stronger plasma recoil pressure, creating a valley in the central region of laser spot. Figure 10 shows scanning path of laser; at first, the laser was scanned parallel to *x*-direction with a pitch of 40 µm; later, laser was scanned in the perpendicular direction with a pitch of 40 µm to form a grid structure. Table 2 shows the laser parameters; to reduce splattering effect due to beam overlap, higher scanning speed was used as compared to 10 kHz laser irradiation. We can observe from Fig. 11 that structures formed in a grid pattern and initial laser scanning seem to dominate the orientation of structure.

4.6 Element analysis of cone

Figure 12 shows EDX results for the elemental distribution of the surface after the formation of conical structures. It was found that the outer layer of cones was mostly made up of silicon, and some carbon and trace of oxygen was also observed. The globular clusters formed on the cone surface at very high fluence have higher oxygen percentage suggesting oxidation of silicon into silicon dioxide. To verify the EDX results, Raman analysis was also performed on the tips of the cone. Raman shift for single crystal silicon is 521 cm^{-1}; however, peak at 519 cm^{-1} was obtained as shown in Fig. 13. This shift could either represent presence of polycrystalline silicon or existence of residual stress. During the process of cone formation, molten material is pushed upwards (elongation) which solidifies rapidly that might cause residual stress; Bradby et al. reported peak shift in a single crystal germanium due to residual stress [29]. Figure 14 shows inside of a cone. We observe a homogeneous solid core enveloped by a thin

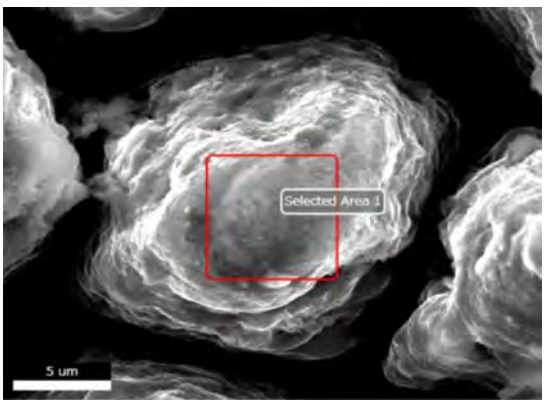

Fig. 12 Tip of cone examined by EDX

Element	Atomic Percentage
Silicon	68.17
Carbon	22.86
Oxygen	7.72

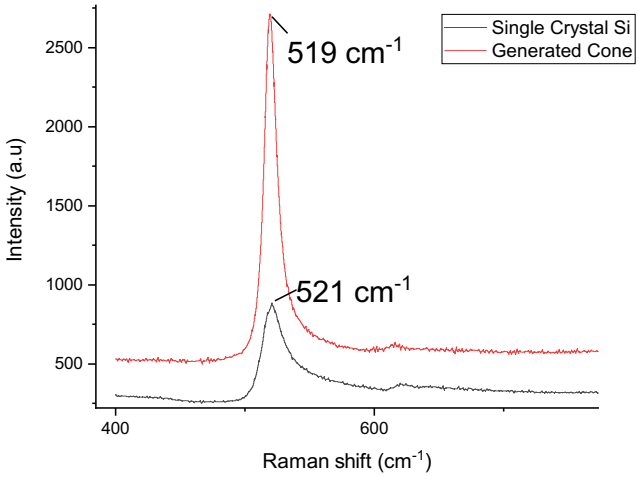

Fig. 13 Raman spectroscopy result for generated cones

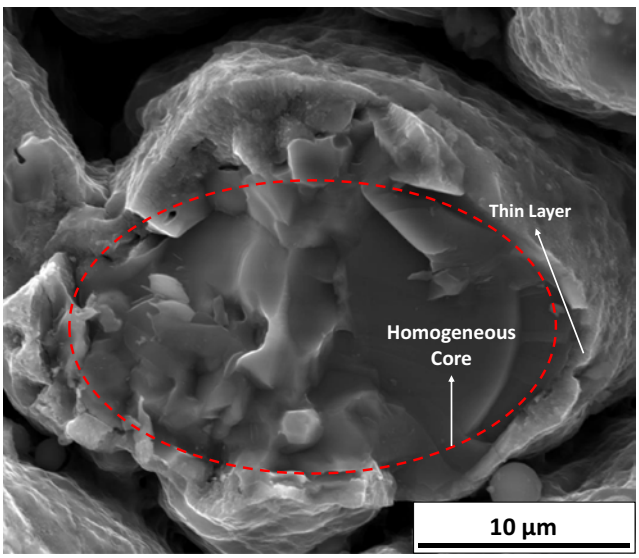

Fig. 14 SEM image of inside of generated cone

layer; EDX reviled both core and the layer is made up of silicon (99%). A possible reason for the formation of thin silicon layer is deposition of vaporized silicon on the cones since laser is scanned multiple times.

4.7 Surface wettability

Wettability of the surface before and after cone generation was measured. The sample was prepared by area irradiation with a laser fluence of 3.17 J/cm^2, laser scan speed of 10 mm/s, and pitch of 10 µm, and the number of scanning repetition was 5. Laser pulse width of 48.4 ns and pulse frequency of 10 kHz were used. A droplet of 5-µL distilled water was used in a static sessile drop method. Figure 15 shows the photograph of water droplet on non-irradiated and irradiated surface. The contact angle of water with non-irradiated sample was measured to be 62° and ~ 0° on irradiated surface, i.e., formation of cone structure made the surface superhydrophilic. This increase in hydrophilicity of the surface suggests that Wenzel state is dominant as water can easily flow between cones, thus increasing the contact area between water and sample surface. Similar shape and size of conical structures (epidermal cells) are also observed on leaves of Calathea zebrina and Ruellia devosiana which are known to be superhydrophilic surfaces [30]. Hence, it is believed that change in contact angle is due to formation cones and not due to change in chemical composition of surface. Such hydrophilic surfaces are especially useful for interface lubrication such as that in applications of bearings and cutting tools.

5 Conclusions

Self-organized microcones with high-number density that protrude well above the initial surface were fabricated on reaction bonded silicon carbide by nanosecond pulsed laser irradiation with a wavelength of 532 nm. It was found that:

(1) Cones are generated as a result of selective melting of silicon initially which is then pushed upwards due to plasma recoil pressure and solidifies rapidly.
(2) As the incident fluence increase, the size of cones increases until a threshold is reached after which the increase in fluence causes ablation. Fluence will determine the surface morphology of the conical structure.
(3) Longer pulse width and higher pulse frequency can melt a large volume of surface and hence can generate larger cones.
(4) Multiple scanning of laser causes ablation of generated cones, splattering material on the surface.
(5) Top layer cones are mostly made up of silicon with some carbon and traces of oxygen. At higher fluence, more silicon is oxidized. Internally cones have a homogeneous core surrounded by an uneven layer.
(6) Generation of cones made the surface superhydrophilic. The contact angle with water became ~ 0°.

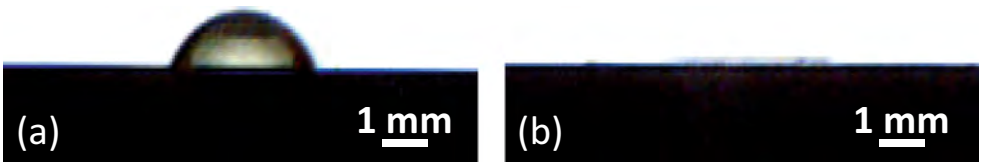

Fig. 15 Photograph showing water droplet on **(a)** original surface **(b)** after cone generation

Further investigation will be carried out to improve the aspect ratio of conical structures. In addition, attempts will be made to fabricate SiC conical structures.

References

1. Suyama S, Itoh Y, Tsuno K, Ohno K (2005) Φ 650 mm optical space mirror substrate of high-strength reaction-sintered silicon carbide. Proc. SPIE:5868. https://doi.org/10.1117/12.616043
2. Toulemont Y, Breysse J, Piepot D, Miura S (2004) The 3.5 m all SiC telescope for SPICA. SPIE 5487:1001–1012. https://doi.org/10.1117/12.551405
3. Xing Y, Deng J, Wu Z, Wu F (2017) High friction and low wear properties of laser-textured ceramic surface under dry friction. Opt Laser Technol 93:24–32. https://doi.org/10.1016/j.optlastec.2017.01.032
4. Murzin SP, Balyakin VB (2017) Microstructuring the surface of silicon carbide ceramic by laser action for reducing friction losses in rolling bearings. Opt Laser Technol 88:96–98. https://doi.org/10.1016/j.optlastec.2016.09.007
5. Geiger M, Roth S, Becker W (1998) Influence of laser-produced microstructures on the tribological behaviour of ceramics. Surf Coatings Technol 100–101:17–22. https://doi.org/10.1016/S0257-8972(97)00581-1
6. Kondrashov V, Rühe J (2014) Microcones and nanograss: toward mechanically robust superhydrophobic surfaces. Langmuir 30:4342–4350. https://doi.org/10.1021/la500395e
7. Li XM, Reinhoudt D, Crego-Calama M (2007) What do we need for a superhydrophobic surface? a review on the recent progress in the preparation of superhydrophobic surfaces. Chem. Soc. Rev. 36:1350–1368
8. Younkin R, Carey JE, Mazur E, Levinson JA, Friend CM (2003) Infrared absorption by conical silicon microstructures made in a variety of background gases using femtosecond-laser pulses. J Appl Phys 93:2626–2629. https://doi.org/10.1063/1.1545159
9. Crouch CH, Carey JE, Warrender JM, Aziz MJ, Mazur E (2004) Comparison of structure and properties of femtosecond and nanosecond laser-structured silicon. Appl Phys Lett 84:1850–1852. https://doi.org/10.1063/1.1667004
10. Bäuerle D (2000) Laser Processing and Chemistry. Springer, Berlin
11. Brown MS, Arnold CB (2010) Fundamentals of laser-material interaction and application to multiscale surface modification. In: Sugioka K, Meunier M, Piqué A (eds) Laser Precision Microfabrication. Springer Series in Materials Science, vol 135. Springer, Berlin, Heidelberg, pp 91–120
12. Ness JN, Page TF (1986) Microstructural evolution in reaction-bonded silicon carbide. J Mater Sci 21:1377–1397. https://doi.org/10.1007/BF00553278
13. Humphreys RG, Signals R, Establishment R et al (1981) ReceDed 22. Energy 39:163–167
14. Philipp HR, Taft EA (1960) Silicon carbide – a high temperature semiconductor. In: O'Connor JR, Smiltens J (eds) . Pergamon Press, Oxford, London, New York, Paris, p 366
15. Groth R, Kauer E (1961) Absorption freier Ladungsträger in CdS. Phys Status Solidi 1:650–655. https://doi.org/10.1002/pssb.19610010609
16. Watanabe N, Kimoto T, Suda J (2014) Temperature dependence of optical absorption coefficient of 4H- and 6H-SiC from room temperature to 300 °C. Jpn J Appl Phys 53:12–15. https://doi.org/10.7567/JJAP.53.108003
17. Choyke WJ, Patrick L (1960) Silicon carbide – a high temperature semiconductor. In: O'Connor JR, Smiltens J (eds) . Pergamon Press, Oxford, London, New York, Paris, p 306
18. Yu G, Levinshtein ME, Rumyantsev SL (2001) Properties of Advanced SemiconductorMaterials GaN, AlN, SiC, BN, SiC, SiGe . Eds. Levinshtein M.E., Rumyantsev S.L., Shur M.S., John Wiley & Sons, Inc., New York. pp 93-148.
19. Duc DH, Naoki I, Kazuyoshi F (2013) A study of near-infrared nanosecond laser ablation of silicon carbide. Int J Heat Mass Transf 65:713–718. https://doi.org/10.1016/j.ijheatmasstransfer.2013.06.050
20. Samant AN, Daniel C, Chand RH, Blue CA, Dahotre NB (2009) Computational approach to photonic drilling of silicon carbide. Int J Adv Manuf Technol 45:704–713. https://doi.org/10.1007/s00170-009-2004-0
21. Fedorenko L, Medvid' A, Yusupov M, Yukhimchuck V, Krylyuk S, Evtukh A (2008) Nanostructures on SiC surface created by laser microablation. Appl Surf Sci 254:2031–2036. https://doi.org/10.1016/j.apsusc.2007.08.048
22. Cappelli E, Orlando S, Mattei G, Montozzi M, Pinzari F, Sciti D (1999) Surface modifications of carbide ceramics induced by pulsed laser treatments. Appl Phys A Mater Sci Process 69:515–519. https://doi.org/10.1007/s003399900329
23. Shigematsu I, Kanayama K, Tsuge A, Nakamura M (1998) Analysis of constituents generated with laser machining of Si3N4and SiC. J Mater Sci Lett 17:737–739. https://doi.org/10.1023/A:1006606810476
24. Bai Y, Li L, Xue D, Zhang X (2016) Rapid fabrication of a silicon modification layer on silicon carbide substrate. Appl Opt 55:5814. https://doi.org/10.1364/ao.55.005814
25. Dutto C, Fogarassy E, Mathiot D (2001) Numerical and experimental analysis of pulsed excimer laser processing of silicon carbide. Appl Surf Sci 184:362–366. https://doi.org/10.1016/S0169-4332(01)00518-9
26. Chen SC, Cahill DG, Grigoropoulos CP (2002) Melting and surface deformation in pulsed laser surface micromodification of Ni-P Disks. J Heat Transfer 122:107. https://doi.org/10.1115/1.521441
27. György E, Mihailescu IN, Serra P, P´erez del pino A, Morenza JL (2002) Crown-like structure development on titanium exposed to multipulse Nd:YAG laser irradiation. Appl Phys A Mater Sci Process. https://doi.org/10.1007/s003390201307, 74, 755, 759
28. Taylor LL, Qiao J, Qiao J (2016) Optimization of femtosecond laser processing of silicon via numerical modeling. Opt. Mater. Express 6:2745–2758. https://doi.org/10.1364/OME.6.002745
29. Bradby JE, Williams JS, Wong-Leung J, Swain MV, Munroe P (2002) Nanoindentation-induced deformation of Ge. Appl Phys Lett 80:2651–2653. https://doi.org/10.1063/1.1469660
30. Koch K, Barthlott W (2009) Superhydrophobic and superhydrophilic plant surfaces: an inspiration for biomimetic materials. Philos Trans R Soc A Math Phys Eng Sci 367:1487–1509. https://doi.org/10.1098/rsta.2009.0022